Validation of an RNase H2 activity assay suitable for clinical screening

Marian Schulz[1,2], Claudia Günther[3], Rayk Behrendt[1,4], Axel Roers[1,5]

1 Institute for Immunology, Medical Faculty Carl Gustav Carus, TU Dresden, Dresden, Germany

2 University Hospital for Children and Adolescents, University of Leipzig, Leipzig, Germany

3 Department of Dermatology, University Hospital Dresden, TU Dresden, Germany

4 Institute of Clinical Chemistry and Clinical Pharmacology, University Hospital Bonn, Germany

5Institute for Immunology, University Hospital Heidelberg, Heidelberg, Germany

Corresponding authors: Axel Roers, axel.roers@tu-dresden.de;
Marian Schulz, marian.s.schulz@gmail.com

Number of text pages: ***33***

Number of tables: **2**

Number of figures: **7**

Number of supplemental tables: **1**

Number of supplemental figures: **2**

Grant numbers, funding: Funded by Deutsche Forschungsgemeinschaft (DFG, German Research Foundation) – Project-ID 369799452 – TRR237 project B17 to A.R., project B19 to R.B. and project B20 to C.G.; and by Else Kröner-Fresenius-Stiftung Grant 060_380627 to M.S.

Financial Disclosure and Conflicts of Interest: The authors declare that there are no conflicts of interests.

Abstract

As the key enzyme mediating ribonucleotide excision repair, RNase H2 is essential for the removal of single ribonucleotides from DNA in order to prevent genome damage. Loss of RNase H2 activity directly contributes to the pathogenesis of autoinflammatory and autoimmune diseases and might further play a role in ageing and neurodegeneration. Moreover, RNase H2 activity is a potential diagnostic and prognostic marker in several types of cancer. Until today, no method for quantification of RNase H2 activity has been validated for the clinical setting. Herein, validation and benchmarks of a FRET-based whole-cell lysate RNase H2 activity assay are presented, including standard conditions and procedures to calculate standardized RNase H2 activity. Spanning a wide working range, the assay is applicable to various human cell or tissue samples with overall methodological assay variability from 8.6% to 16%. The assay readily detected reduced RNase H2 activity in lymphocytes of a patient with systemic sclerosis carrying a *RNASEH2C* variant. Implementation of larger control groups will help to assess the diagnostic and prognostic value of clinical screening for RNase H2 activity in the future.

Introduction

An increasing number of inflammatory and degenerative diseases are found to be associated with compromised genome integrity. In some of these, genome damage is assumed to be a central pathogenic event, while in others DNA damage may represent an epiphenomenon [1–5]. Resolution of RNA/DNA hybrids is central to various DNA transactions and maintenance of genome integrity. Mammals express RNases H1 and H2 which both cleave RNA/DNA hybrids by catalysing phosphodiester bond hydrolysis [6]. The enzymes play a role in resolution of R-loops, maturation of Okazaki fragments, repression of endogenous retroelements and degradation of RNA/DNA hybrids during cell death [7–9]. While RNase H1 requires hybrids with at least 2 consecutive ribonucleotides, RNase H2 also cleaves single ribonucleotides embedded in the DNA double helix [10]. Ribonucleotides are incorporated into genomic DNA in very high numbers during replication due to the limited capacity of the replicative polymerases to discriminate them from desoxyribonucleotides (Lujan et al., 2013; Sassa et al., 2019). To prevent destabilization of DNA, ribonucleotides are rapidly removed post-replication by the ribonucleotide excision repair (RER) pathway initiated by RNase H2-mediated nicking 5' of the ribonucleotide. RER is the only error-free pathway capable of removing single ribonucleotides from DNA [7–9]. Failure to repair these lesions leads to DNA damage [8,11–16]. In mammals, complete loss of RNase H2 activity leads to embryonic lethality [12,14]. Partial loss of function, however, caused by hypomorphic *RNASEH2* alleles can lead to autoinflammation and autoimmunity, as for example in Aicardi-Goutières syndrome (AGS), a monogenic 'type I interferonopathy' [17–19]. Hypomorphic *RNASEH2* alleles also contribute to the polygenic predisposition for systemic lupus erythematosis (SLE) [20–22]. Investigation of RNase H2-deficient human cells and mice recently led to elucidation of an important link between genome damage and chronic inflammation [12]. DNA lesions ensuing from unrepaired ribonucleotides result in chromosomal aberrations, problems of mitotic segregation of defective chromosomes and formation of micronuclei. Upon collapse of the unstable micronuclear envelope, micronuclear chromatin is sensed by the intracellular DNA sensor cGAS, in turn resulting in activation of the sensor STING and activation of type I IFN and

proinflammatory cytokine responses [23–25]. Chronic activation of cGAS/STING signalling leads to autoinflammation, loss of T cell and B cell tolerance and autoimmune pathology [18]. RNase H2 deficiency also predisposes to cancer in mice [26,27] and RNase H2 loss-of-function mutations occur in large fractions of human chronic lymphocytic leukaemia and prostate cancer [28]. Reduced expression of RNase H2 is associated with reduced survival in colonic cancer [27]. Conversely, upregulation of RNase H2 subunits was found to be a malignancy factor in numerous carcinomas and sarcomas [29–31]. Moreover, double-strand breaks as resulting from compromised RNase H2 function were reported to contribute to neurodegeneration and aging [32–34]. Collectively, RNase H2 is a relevant diagnostic and prognostic factor in diverse human disease settings, warranting clinical testing for RNase H2 activity in human cells or tissues.

Human RNase H2, unlike its monomeric prokaryotic isoenzyme RNase HII, is a heterotrimeric complex consisting of three proteins, the catalytic subunit RNase H2A and two auxiliary subunits, RNase H2B and RNase H2C [35–37]. About 50 disease-causing *RNASEH2* variants have been identified to date [21,22,24,38], most of which are located in subunit B. While many variants exibit reduced RNase H2 substrate binding and hydrolysis, other mutant proteins did not show impaired activity in cell free assays using recombinant enzyme [39]. The latter might feature compromized complex stability or interaction with additional proteins *in vivo*.

Although measurement of RNase H activity in mammalian cell samples has been performed since it's discovery in 1969 [40], a standardized and validated method available for clinical use has been lacking. RNase H activity can be quantified by several different approaches relying on acid-insoluble precipitation, gel electrophoresis or HPLC. Two groups developed a fluorescence assay suitable for high-throughput studies and superior to earlier approaches with respect to precision, speed, labour and cost. RNase H2-mediated cleavage of a double-stranded DNA substrate containing a single ribonucleotide results in release of a fluorescein-labelled fragment from a quencher [41,42]. Herein, we adapt this assay into a standardized and

validated procedure relying on whole cell lysates for clinical screening of effective intracellular RNase H2 activity.

Materials and Methods:

Ethics approval and control group selection

Ethics approval was granted by the ethics committee of the Medical Faculty Carl Gustav Carus, TU Dresden (EK 31022012). Volunteers older than 18 years of age without overt disease for the past two weeks were included after informed consent. Pregnancy or medication, abuse of alcohol or drugs were exclusion criteria. Volunteers did not receive financial or other compensation.

Cell culture

HeLa cells and murine embryonic fibroblasts (MEFs) were cultured in Gibco® DMEM – Dulbecco's Modified Eagle Medium (Fisher Scientific GmbH, Schwerte, Germany) at 37 °C and 5% CO_2. For harvesting, medium was aspirated, adherent cells were washed twice with 1x PBS followed by incubation with 1x trypsin (0.25%, Life Technologies Germany, Darmstadt, Germany) at 37°C for 2 minutes. Digest was stopped by addition of FCS-containing medium, cells were detached by pipetting, transferred into a 15-ml conical tube and pelletted at 330 x g for 5 min. Cells were resuspended, washed twice in 5 ml of chilled PBS for freezing, or in 1x FACS buffer for FACS sorting. For freezing, supernatant was discarded, pellets were shock-frozen in liquid nitrogen and then stored at -80°C for a maximum of 4 weeks.

Isolation of Primary cells from human blood and mice

For isolation of human PBMC, peripheral blood was collected in 10 ml heparinized tubes, stored at 4°C and analysed within 4 hours. Blood was diluted in an equal volume of PBS (calcium- and magnesium-free, equilibrated to room temperature (RT)). PBMC were isolated by standard Ficoll®-Paque density gradient centrifugation, and washed 3 times with chilled PBS. Murine keratinocytes, peritoneal cells, splenocytes and embryonic fibroblasts were isolated by standard procedures [43–46]

Flow cytometric cell sorting

PBMC from human donors were stained with anti-human CD3 (UCHT1) PE and anti-human CD19 (SJ25-C1) APC-H7, murine spleen cells with anti-CD19 (eBio1D3) PE, anti-CD4 (RM4-5) APC, anti-CD11b (M1/70) eF450 and anti-CD11c (N418) PE/Cy7, murine peritoneal lavage cells with anti-CD11b (M1/70) eF450 and anti-F4/80 (BM8) PE, and murine epidermal cells with anti-CD49f (eBioGoH3 rat) PE antibodies at 4°C for 30 minutes. Antibodies were purchased from Thermo Fisher Scientific Germany (Frankfurt a. M., Germany). Stained cells, or harvested cell culture cells, respectively, were washed with FACS buffer three times and resuspended in FACS buffer. Shortly before analysis, DAPI was added to a final concentration of 3 µM. Cells were sorted on a BD FACSAria™ III (Beckton Dickinson Germany, Heidelberg, Germany) excluding doublets and dead cells. Data was analyzed using FlowJo Single Cell Analysis Software (FLOWJO, LLC Data analysis software).

Cell lysis and protein quantification

Washed cell pellets were dissolved in a suitable amount of lysis buffer 1 and incubated on ice for 10 min. After addition of the same amount of lysis buffer 2 and another incubation on ice for 10 minutes, cell debris was spun down at 20 000 x g for 10 min at 4°C. Supernatant containing total cellular protein was harvested, and replicates were stored at -80°C. Protein concentration was determined using the Qubit™ Protein Assay Kit (ThermoFisher scientific) following recommendations of the vendor.

RNase H2 activity assay and standard conditions

RNase H2 activity was measured using a fluorometric assay approach adapted from Crow et al. (Crow et al., 2006). The type 2 RNase H-specific substrate consisted of an 18 bp DNA strand containing a single ribonucleotide 4 bp 5' of a covalently attached 3' fluorescein residue (oligonucleotide B) which was annealed to a 18 bp anti-sense DNA strand with a quenching 5' dabcyl residue (oligonucleotide D). Type 2 RNase H hydrolyses the phosphodiester bond 5' of the single ribonucleotide leading to dissociation of the fluorescein-carrying fragment from the quencher allowing photometric quantification (Figure 1A). As

positive controls, unquenched single-stranded substrate (B), unquenched double-stranded substrate lacking the dabcyl residue at the anti-sense strand (BK), and plateau-fluorescence of the fluorescence progress curve (BD plateau), were implemented. BD plateau-fluorescence was determined by measuring fluorescence in wells containing 100 eqU HeLa RNase H2 and different amounts of substrate BD for 270 min until there was no further fluorescence increase. The mean of the last three measurement value triplicates was defined as BD plateau-fluorescence. As negative controls, quenched type 2 RNase H-specific substrate without addition of RNase HII (BD), quenched type 2 RNase H-specific substrate with addition of *heat-inactivated* cell lysate (BD + *h.i. lysate*), quenched double-stranded 2-O'-methylated RNA / DNA (type 2 RNase H-resistant) substrate (AD) with addition of active RNase HII, and blanks, were used. Desalted oligonucleotides were purchased from Eurogentec (Seraing, Belgium), dissolved in TE buffer to a final concentration of 100 µM and annealed by heating to 90 °C for 2 minutes and then gradually cooling down by 1 °C per minute. Then, substrates were aliquoted and stored at -20 °C at a concentration of 10 pmol / µl.

After cell isolation, cell number or protein content was quantified and cell pellets were lysed as described above. Cell lysates were premixed on ice with an 1 : 1 mixture of lysis buffer 1 and 2 in a 96-well flat-bottomed plate. Then, equal amounts of cell lysate premixes were pipetted to another flat-bottomed 96-well reaction plate containing 100 µl reaction buffer with 270 nM type 2 RNase H-specific substrate (BD) using a multi-channel pipette. The reaction was monitored in a FLUOstar® Omega photometer at 37 °C for at least 120 min, fluorescence was measured at 3 minute intervals. Before measurement, the photometer was calibrated, setting the 30 nM unquenched single-stranded substrate B positive control fluorescence to 33333 FU. Photometer measurement range was set to 100 %. A 485 nm excitation filter and a 520 nm emission filter were used. Before each measurement, wells were mixed by orbital shaking (3 mm diameter, 5 s). Fluorescence was induced by 10 flashes per well and cycle, and measurement was performed by orbital scanning by a vertically adjusted sensor. Fluorescence was measured using a time-resolved approach with

an integration delay of 47 µs and an integration time of 1510 µs. Positioning delay was set to 0.2 s, measurement start time to 0.5 s. All assay steps except from photometric measurement were carried out on ice.

Fluorescence data was converted into the equivalent amount of cleaved substrate BD using the BD plateau fluorescence standard curve to acquire substrate cleavage progress curves. The cleavage rate was obtained by linear regression of the curves between minute 3 and 24 (at least 5 data points). Using six quality controls with known activity and the substrate conversion standard curve (Figure 2D), cleavage rates were transformed into standardized catalytic activities (1 “eqU” = equivalent to the catalytic activity of 1 U RNase HII (NEB ®) under standard conditions). To correct for systematic error between different RNase H2 assays, six internal standards (cell lysate aliquots with known RNase H2 activity) were measured in each experiment. For oligonucleotide sequences and buffer reagents, see Table 1 and Table 2.

Statistics

Statistical tests were performed using GraphPad Prism™ 5.04 (GraphPad Software Inc., San Diego, California, USA). Sample size calculations (two-sample t-test) were conducted as proposed by Hulley et al. [47] using G*Power Version 3.1.9.4 © (Franz Faul, Kiel, Germany).

Results

Validation and benchmarks of the RNase H2 activity assay

The assay principle was adapted from Crow et al. [42] as illustrated in Figure 1A. A double-stranded DNA oligonucleotide containing a single ribonucleotide and a fluorescent label (fluorescein) at the 3' end of the same strand were used as a type 2 RNase H-specific substrate. This substrate is cleaved by mammalian RNase H2, but also by bacterial RNase HII. Fluorescence was quenched by a dabcyl-group coupled to the 5' end of the complementary strand. Upon RNase H2-mediated cleavage at the position of the ribonucleotide, a short oligonucleotide carrying the fluorescein label is released from the quencher and fluorescence is quantified by photometry.

Implementation of controls and standard curves

Figure 1B shows fluorescence progress curves for type 2 RNase H-specific (BD) and control substrates (B, BK, AD, see Figure 1A). Bacterial RNase HII cleaved substrate BD with fluorescence reaching a plateau (Figure 1B), while this substrate showed only weak spontaneous background fluorescence (6.06% of plateau level). Spontaneous dequenching by degradation of quenched substrate BD was insignificant (Figure 1B). Addition of heat-inactivated cell lysate had no effect on fluorescence, indicating absence of unspecific (heat-sensitive) quenchers. Likewise, there was no unspecific substrate degradation detectable upon addition of active cell lysate to type 2 RNase H-resistant substrate AD (Figure 1B). Maximum fluorescence of fully cleaved substrate BD (BD plateau fluorescence) was defined as high control for substrate conversion.

To allow inter-laboratory reproducibility, the assay was validated using E. coli RNase HII with standardized activity. Different amounts of RNase HII were added to samples containing substrate BD and fluorescence progress curves (results for 55 U and 100 U RNase HII shown in Fig. 1B) were determined in pipetting triplicates under standard assay conditions. Fluorescence progress curves were double-curved exhibiting a significant lag phase. This was unexpected for a pseudo-first order irreversible reaction with a single substrate and

without any known inhibitors or any described conformational changes of the enzyme during the reaction [48,49]. Therefore, it was hypothesized, that this lag phase was due to non-linear, concentration-dependent fluorescence behaviour of the fluorophore. Indeed, implementation of a positive control fluorescence standard curve by enzymatic dequenching of substrates BD and B demonstrated fluorescence non-linearity of the fluorophore (Figure 1C). We therefore converted fluorescence data into amount of cleaved substrate based on the fluorescence standard curve (Figure 1C). Increase of amount of cleaved substrate over time showed perfectly linear behaviour without a significant lag phase (Figure 1D) allowing for definition of the steady-state phase, in which linear regression was performed to calculate RNase H2 activity. Linearity was highly significant with an r square value of >0.99 for all curves corresponding to RNase HII activity above 8.09 U (limit of quantification (LOQ), see below). Hence, steady state conditions could be assumed for enzyme activities between 8.09 and 200 U of E. coli RNase HII under standard conditions.

Substrate B positive control fluorescence was used for photometer calibration to ensure reproducibility of experimental data. Plotting catalytic activities of standardized amounts of RNase HII yielded a substrate conversion standard curve (Figure 1E). Using this standard curve, measured catalytic activity was converted into the equivalent activity (“eqU”) of a defined amount of externally validated reference-RNase HII. Substrate conversion rates showed no significant deviation from linearity in the validated working range indicating small systematic error as well as absence of activators or inhibitors in the reaction mix.

For comparison and combination of data from different RNase H2 assays, internal standards (see Materials and Methods) were used. *Inter*-assay systematic error was assessed between three individual RNase H2 activity assays using aliquots of the same mouse embryonic fibroblast lysate. Means differed by 3.65% (SD=1.78; n=3). However, the precision by which this systematic error was calculated was strongly dependent on the number of matched quality controls established between the individual assays (Figure 1F). Use of six matched quality controls reduced variability of the calculation of systematic error to less than 3%.

Sensitivity and ruggedness

The average curve slope of substrate BD without addition of enzyme was 7.8 fluorescence units (FU) per minute (0.026 % of positive control fluorescence, calculated from data shown in Figure 1B). This was equivalent to a substrate cleavage rate of 5.4 fmol/min resulting in a limit of detection (LOD) of 9.7 fmol/min (2.09 eqU) and an LOQ of 32.3 fmol/min (8.09 eqU) [50].

Designing the RNase H2 assay for high-throughput analysis required prolonged sample handling and sample storage. Systematic sample handling error was assessed by subjecting HeLa whole cell lysate to repeated freezing and thawing (Figure 2A) or by incubation at RT for defined time (Figure 2B). Each freeze-thaw cycle reduced RNase H2 activity by 0.37eqU (4.5% of LOQ). Likewise, incubation at RT reduced enzyme activity at a rate of 0.53 eqU per hour (6.6% of LOQ).

Standard sample handling involved one freeze-thaw cycle and incubation times between 30 minutes and 2 hours, which were, however, performed on ice rather than RT, suggesting maximal loss of RNaseH2 activity of 1.43 eqU (17.7 % of LOQ) due to the processing.

Steady-state kinetics and assay endpoints

In search for the most-suited parameter to be determined (assay endpoint) for purposes of clinical screening, RNase H2 steady-state kinetics was studied. For this, 2.5 µg of HeLa protein (30 eqU) were added to wells containing eight different substrate concentrations spread around the expected K_M-value [6,51]. This was performed with HeLa protein from six individual HeLa cell cultures. Michaelis-Menten curves were determined using the initial-rates method and Michaelis-Menten non-linear regression (Figure 3). RNase H2 activity followed Michaelis-Menten kinetics with a mean K_M of 141.7 nM and a high mean C_V of 65.72 %. Calculation of V_{MAX} was less variable with a mean C_V of 24.45%. Still, highest precision was obtained by measuring RNase H2 activity at a single substrate concentration (provided a substrate concentration >2SD above K_M was used). At a substrate concentration of 270 nM, RNase H2 activity reached approximately 60% of V_{MAX} and measurement variability was

below 10%. Higher substrate concentrations lead to a systematic distortion of RNase H2 activity due to non-linear fluorescence behaviour of the fluorophores (Figure 1C). Therefore, it was concluded, that RNase H2 activity at a substrate concentration of 270 nM was best-suited as assay endpoint for purposes of clinical screening.

Precision

Overall precision was determined for the assay based on primary or cultured cells. Hereby, the influence of different assay steps (cell isolation and preparation, pipetting, photometric measurement and linear regression) and normalization methods (normalization to cell number or total protein) on overall variability was assessed. Total assay variability including all biological and methodological error sources ranged from 8.6% to 16% (C_V).

Variability due to linear regression, photometer imprecision or pipetting was assessed in an experiment with 105 pipetting replicates and averaged at 7.73 %. This accounted for more than half of total assay variability (56.2 %; 95 % CI = 14.7 % - 97.8 %, n = 4), depending on the experimental approach and normalization method (contribution of single error sources on the total coefficient of variation was calculated using addition of variances). Under standard conditions, the largest part of this methodological error was attributed to pipetting error, while linear regression and photometer imprecision constituted minor error sources (not shown). Assay precision was strongly dependent on the normalization method used. Experiments relying on normalization to total protein avaraged a total assay variability of 9.6 %, unaffected by the cell isolation method (FACS-sorting or direct lysis of cultured cells), while normalization to cell number resulted in a much larger total assay variability of 16 % (Figure 4). We attributed this primarily to loss of cells during washing steps and, less predominantly, imprecisions of FACS cell counting. Isolation of primary cells from peripheral blood by Ficoll gradient centrifugation is known to yield PBMCs of variable cell type composition and viability [52,53]. Thus, isolation of primary blood cells resulted in higher overall variability (11.17 %) than direct lysis of cultured cells.

304 **Screening RNase H2 activity in human lymphocytes**

305 RNase H2 activity differed significantly between cell types (Figure 5). In mouse cells, RNase
306 H2 activity changed with cell cycle phase (Supplemental Figure S2). To reduce variability, we
307 aimed to assay for enzyme activity in one particular cell type rather than in samples
308 containing undefinded mixtures of different cells. We chose to base the assay on
309 lymphocytes as they are easily obtained in large numbers from blood and feature high
310 RNase H2 activity (Figure 5 and Supplemental Table S1). PBMCs were obtained from blood
311 samples of 24 healthy donors (Supplemental Figure S1) with unknown *RNASEH2* genotypes
312 by FICOLL® gradient centrifugation. $CD19^+$ B cells and $CD3^+$ T cells were isolated by flow
313 cytometric sorting. From a 10 ml blood sample, 4.0×10^5 B cells and 3.0×10^6 T cells were
314 obtained, sufficient for multiple replicate measurements (Supplemental Table S1). Control
315 group size was designed to allow detection of a reduction of RNase H2 activity by 30 % with
316 a statistical power of 90 % and α of 0.10.
317 In T cells, RNase H2 activity per µg of cellular protein was about 3-fold higher than in B cells
318 (Figure 6B), while RNase H2 activity per cell did not differ significantly between B and T cells
319 (Figure 6C), reflecting higher total protein content of B cells compared to T cells. *Inter*-
320 individual assay variability in T cells was approximately four-fold lower as in B cells,
321 irrespective of the normalization method (Fig. 6D).
322 In T cells, *inter*- and *intra*-individual variability did not differ significantly. When activity was
323 measured in T cells with normalization to cell numbers, the highest error source was
324 methodological variability. In B cells, however, *inter*-individual variability clearly exceeded
325 *intra*-individual and methodological variability. Gender and age did not contribute to *inter*-
326 individual variability (not shown).
327 Collectively, we show that quantification of RNase H2 activity in T cells requires small
328 amounts of venous blood and shows little *inter*-individual and *intra*-individual variation
329 making it a suitable method for clinical use.

***RNASEH2C c.468G>T* reduces RNase H2 activity in T cells**

A pilot experiment was performed on a systemic sclerosis patient carrying an *RNASEH2C* variant with so far unknown effects on RNase H2 activity (c.468G>T, rs61736590). The condition of this 60-year old female was classified as 'limited disease' (onset with 33 years) with antinuclear antibodies (titre 1:2560, Scl 70), Raynaud's syndrome, mutilation of finger tips by digital ulcers at onset of the disease, lung fibrosis and oesophageal involvement. She received no immunomodulatory or immunosuppressive therapy. The heterozygous mutation in *RNASEH2C* was identified by whole exome sequencing and verified by Sanger sequencing of DNA from PBMCs (Figure 7A). RNase H2 activity measured in triplicate samples was compared to the group of healthy controls (n = 24, Supplemental Figure S1) using unpaired two-tailed t-tests with Welch's correction. RNase H2 activity per cell was significantly reduced in the patient's T cells compared to the control group. Residual activity per cell and per µg of cellular protein in T cells was 80 % and 63.5 % of control activity, respectively (Figure 7B-D). Collectively, our data show that the assay readily detected the reduction of RNase H2 activity caused by the heterozygous *RNASEH2 c.468G>T* variant.

346 ***Discussion:***

347 We present standardization and validation of an assay allowing for quantification of RNase
348 H2 activity in cell lysates. The assay is based on the experimental procedure published by
349 Crow et al [42], and is suitable for screening of clinical samples. Measurement of RNase H2
350 activity has primarily been performed on recombinant wild type or mutant RNase H2
351 [6,12,35,36,54]. Assays based on recombinant protein have important limitations as effects of e.g.
352 protein stability or protein-protein interaction are not captured. Recombinant protein
353 expression requires sequencing and cloning of gene variants, precluding adaptation to
354 settings of clinical screening. Assays involving overexpression of recombinant proteins also
355 do not address effects of intracellular expression levels of functional enzyme. We directly
356 measure RNase H2 activity of cell lysates, enabling determination of enzyme activity per cell
357 or per amount of cellular protein, capturing any effect on levels of functional enzyme in the
358 cell, including alteration of transcription, posttranscriptional regulation, posttranslational
359 modifications and protein stability.
360 While the assay is based on lymphocytes sorted by FACS in the present study, less
361 sophisticated methods of cell separation are clearly sufficient. In contrast to flow cytometric
362 sorting, immunomagnetic cell separation [55], is cost- and labor-efficient, requires only simple
363 equipment, and allows fast enrichment of B or T cells from peripheral blood samples to high
364 purity. Future establishment of a larger and more heterogeneous control cohort evenly
365 distributed between all age groups and gender is necessary to identify potential confounders
366 (e.g. ethnicity, hormonal changes, medication, stress, circadian rhythm, CD4+/CD8+ ratio,
367 etc.) contributing to *inter*- and *intra*-individual variability. While the assay enables reliable
368 detection of activity reduction by 30% comparing triplicate measurements of a single sample
369 to the control group mean (24 individuals), increasing replicate measurements of patient
370 samples to 5 and control cohort size to 100 would improve the minimal detectable activity
371 reduction to 20%, which is in the range of inter-individual variability. Therefore, an activity
372 reduction of less than 20% is unlikely to be clinically relevant. Measurement of RNase H2
373 activity in triplicate T cell samples from a patient suffering from systemic sclerosis revealed

significantly reduced activity by normalization to cell number or to amount of total cellular protein. Since RNase H2 is a nuclear protein and genomic DNA is its substrate, and cell volume the activity per genome, i.e. per cell, seems to be the most important parameter, while cellular volume and protein content are subject to fluctuations, e.g. depending on the cell cycle (Supplemental Figure S2). The assay is fully standardized and externally validated quality controls meeting all requirements for certified reference materials were implemented ensuring inter-laboratory reproducibility. High sensitivity, robustness against impact of sample storage or freezing and a broad working range enable versatile applications.

Collectively, we provide a fully standardized, validated and benchmarked assay suitable for quantification of RNase H2 enzyme activity in clinical cell samples. The assay is sensitive and precise. It revealed differences in RNase H2 activity dependent on cell type and cell cycle phase as well as the reduction of enzyme activity caused by a heterozygous RNASEH2C partial loss-of-function mutation. The assay will be valuable for screening clinical entities for alterations of RNase H2 function in autoimmunity and cancer.

Acknowledgements

We thank Barbara Utess, Livia Schulze, Christina Hiller and Christa Haase for excellent technical support, Björn Hiller for help with the isolation of primary cells. iPS cells were kindly provided by Michael Haase, Department of Pediatric Surgery, Medical Faculty, TU Dresden. This work was funded by the Deutsche Forschungsgemeinschaft (DFG, German Research Foundation) – Project-ID 369799452 – TRR237 Nucleic Acid Immunity, project B17 to A.R., project B19 to R.B. and project B20 to C.G., as well as by Else Kröner-Fresenius-Foundation grant 060_380627 to M.S.

References

1. Gustafson MA, Sullivan ED, Copeland WC. Consequences of compromised mitochondrial genome integrity. DNA Repair (Amst), 2020, 93:102916
2. McKinnon PJ. Genome integrity and disease prevention in the nervous system. Genes Dev, 2017, 31:1180–94
3. Jackson SP, Bartek J. The DNA-damage response in human biology and disease. Nature, 2009, 461:1071–8
4. Chow HM, Herrup K. Genomic integrity and the ageing brain. Nat Rev Neurosci, 2015, 16:672–84
5. Madabhushi R, Pan L, Tsai LH. DNA damage and its links to neurodegeneration. Neuron, 2014, 83:266–82
6. Rohman MS, Koga Y, Takano K, Chon H, Crouch RJ, Kanaya S. Effect of the disease-causing mutations identified in human ribonuclease (RNase) H2 on the activities and stabilities of yeast RNase H2 and archaeal RNase HII. FEBS J, 2008, 275:4836–49
7. Heider MR, Burkhart BW, Santangelo TJ, Gardner AF. Defining the RNaseH2 enzyme-initiated ribonucleotide excision repair pathway in Archaea. J Biol Chem, 2017, 292:8835–45
8. Kellner V, Luke B. Molecular and physiological consequences of faulty eukaryotic ribonucleotide excision repair. EMBO J, 2020, 39:e102309
9. Feng S, Cao Z. Is the role of human RNase H2 restricted to its enzyme activity? Prog Biophys Mol Biol, 2016, 121:66–73
10. Tannous E, Kanaya E, Kanaya S. Role of RNase H1 in DNA repair: removal of single ribonucleotide misincorporated into DNA in collaboration with RNase H2. Sci Rep, 2015, 5:9969
11. Noy A, Pérez A, Lankas F, Javier Luque F, Orozco M. Relative flexibility of DNA and RNA: A molecular dynamics study. J Mol Biol, 2004, 343:627–38
12. Reijns MAM, Rabe B, Rigby RE, Mill P, Astell KR, Lettice LA, Boyle S, Leitch A, Keighren M, Kilanowski F, Devenney PS, Sexton D, Grimes G, Holt IJ, Hill RE, Taylor

426 MS, Lawson KA, Dorin JR, Jackson AP. Enzymatic removal of ribonucleotides from
427 DNA is essential for mammalian genome integrity and development. Cell, 2012,
428 149:1008–22
429 13. Williams JS, Lujan SA, Kunkel TA. Processing ribonucleotides incorporated during
430 eukaryotic DNA replication. Nat Rev Mol Cell Biol, 2016, 17:350–63
431 14. Hiller B, Achleitner M, Glage S, Naumann R, Behrendt R, Roers A. Mammalian RNase
432 H2 removes ribonucleotides from DNA to maintain genome integrity. J Exp Med, 2012,
433 209:1419–26
434 15. MacKenzie KJ, Carroll P, Martin CA, Murina O, Fluteau A, Simpson DJ, Olova N,
435 Sutcliffe H, Rainger JK, Leitch A, Osborn RT, Wheeler AP, Nowotny M, Gilbert N,
436 Chandra T, Reijns MAM, Jackson AP. CGAS surveillance of micronuclei links genome
437 instability to innate immunity. Nature, 2017, 548:461–5
438 16. Sassa A, Yasui M, Honma M. Current perspectives on mechanisms of ribonucleotide
439 incorporation and processing in mammalian DNA. Genes Environ, 2019, 41:3
440 17. Crow YJ, Manel N. Aicardi-Goutières syndrome and the type I interferonopathies. Nat
441 Rev Immunol, 2015, 15:429–40
442 18. Lee-Kirsch MA, Wolf C, Kretschmer S, Roers A. Type I interferonopathies—an
443 expanding disease spectrum of immunodysregulation. Semin Immunopathol, 2015,
444 37:349–57
445 19. Volpi S, Picco P, Caorsi R, Candotti F, Gattorno M. Type I interferonopathies in
446 pediatric rheumatology. Pediatr Rheumatol, 2016, 14:1–12
447 20. Crow YJ, Rehwinkel J. Aicardi-Goutie'res syndrome and related phenotypes: Linking
448 nucleic acid metabolism with autoimmunity. Hum Mol Genet, 2009, 18:130–6
449 21. Lee-Kirsch MA, Wolf C, Günther C. Aicardi-Goutières syndrome: A model disease for
450 systemic autoimmunity. Clin Exp Immunol, 2014, 175:17–24
451 22. Günther C, Kind B, Reijns MAM, Berndt N, Martinez-Bueno M, Wolf C, Tüngler V,
452 Chara O, Lee YA, Hübner N, Bicknell L, Blum S, Krug C, Schmidt F, Kretschmer S,
453 Koss S, Astell KR, Ramantani G, Bauerfeind A, Morris DL, Graham DSC, Bubeck D,

454 Leitch A, Ralston SH, Blackburn EA, Gahr M, Witte T, Vyse TJ, Melchers I, Mangold
455 E, Nöthen MM, Aringer M, Kuhn A, Lüthke K, Unger L, et al. Defective removal of
456 ribonucleotides from DNA promotes systemic autoimmunity. J Clin Invest, 2015,
457 125:413–24
458 23. Mackenzie KJ, Carroll P, Lettice L, Tarnauskaitė Ž, Reddy K, Dix F, Revuelta A,
459 Abbondati E, Rigby RE, Rabe B, Kilanowski F, Grimes G, Fluteau A, Devenney PS,
460 Hill RE, Reijns MA, Jackson AP. Ribonuclease H2 mutations induce a cGAS / STING -
461 dependent innate immune response. EMBO J, 2016, 35:831–44
462 24. Pokatayev V, Hasin N, Chon H, Cerritelli SM, Sakhuja K, Ward JM, Douglas Morris H,
463 Yan N, Crouch RJ. RNase H2 catalytic core Aicardi-Goutières syndrome-Related
464 mutant invokes cGAS-STING innate immunesensing pathway in mice. J Exp Med,
465 2016, 213:329–36
466 25. Bartsch K, Knittler K, Borowski C, Rudnik S, Damme M, Aden K, Spehlmann ME, Frey
467 N, Saftig P, Chalaris A, Rabe B. Absence of RNase H2 triggers generation of
468 immunogenic micronuclei removed by autophagy. Hum Mol Genet, 2017, 26:3960–72
469 26. Hiller B, Hoppe A, Haase C, Hiller C, Schubert N, Müller W, Reijns MAM, Jackson AP,
470 Kunkel TA, Wenzel J, Behrendt R, Roers A. Ribonucleotide excision repair is essential
471 to prevent squamous cell carcinoma of the skin. Cancer Res, 2018, 78:5917–26
472 27. Aden K, Bartsch K, Dahl J, Reijns MAM, Esser D, Sheibani-Tezerji R, Sinha A,
473 Wottawa F, Ito G, Mishra N, Knittler K, Burkholder A, Welz L, van Es J, Tran F,
474 Lipinski S, Kakavand N, Boeger C, Lucius R, von Schoenfels W, Schafmayer C, Lenk
475 L, Chalaris A, Clevers H, Röcken C, Kaleta C, Rose-John S, Schreiber S, Kunkel T,
476 Rabe B, Rosenstiel P. Epithelial RNase H2 Maintains Genome Integrity and Prevents
477 Intestinal Tumorigenesis in Mice. Gastroenterology, 2019, 156:145-159.e19
478 28. Zimmermann M, Murina O, Reijns MAM, Agathanggelou A, Challis R, Tarnauskaite Ž,
479 Muir M, Fluteau A, Aregger M, McEwan A, Yuan W, Clarke M, Lambros MB,
480 Paneesha S, Moss P, Chandrashekhar M, Angers S, Moffat J, Brunton VG, Hart T, De
481 Bono J, Stankovic T, Jackson AP, Durocher D. CRISPR screens identify genomic

ribonucleotides as a source of PARP-trapping lesions. Nature, 2018, 559:285–9

29. Mottaghi-Dastjerdi N, Soltany-Rezaee-Rad M, Sepehrizadeh Z, Roshandel G, Ebrahimifard F, Setayesh N. Identification of novel genes involved in gastric carcinogenesis by suppression subtractive hybridization. Hum Exp Toxicol, 2015, 34:3–11

30. Flanagan JM, Funes JM, Henderson S, Wild L, Carey N, Boshoff C. Genomics screen in transformed stem cells reveals RNASEH2A, PPAP2C, and ADARB1 as putative anticancer drug targets. Mol Cancer Ther, 2009, 8:249–60

31. Williams KA, Lee M, Hu Y, Andreas J, Patel SJ, Zhang S, Chines P, Elkahloun A, Chandrasekharappa S, Gutkind JS, Molinolo AA, Crawford NPS. A Systems Genetics Approach Identifies CXCL14, ITGAX, and LPCAT2 as Novel Aggressive Prostate Cancer Susceptibility Genes. PLoS Genet, 2014, 10:e1004809

32. White RR, Vijg J. Do DNA Double-Strand Breaks Drive Aging? Mol Cell, 2016, 63:729–38

33. Zhu L-S, Wang D-Q, Cui K, Liu D, Zhu L-Q. Emerging Perspectives on DNA Double-strand Breaks in Neurodegenerative Diseases. Curr Neuropharmacol, 2019, 17:1146–57

34. Storci G, De Carolis S, Papi A, Bacalini MG, Gensous N, Marasco E, Tesei A, Fabbri F, Arienti C, Zanoni M, Sarnelli A, Santi S, Olivieri F, Mensà E, Latini S, Ferracin M, Salvioli S, Garagnani P, Franceschi C, Bonafè M. Genomic stability, anti-inflammatory phenotype, and up-regulation of the RNAseH2 in cells from centenarians. Cell Death Differ, 2019, 26:1845–58

35. Rychlik MP, Chon H, Cerritelli SM, Klimek P, Crouch RJ, Nowotny M. Crystal structures of rnase h2 in complex with nucleic acid reveal the mechanism of RNA-DNA junction recognition and cleavage. Mol Cell, 2010, 40:658–70

36. Shaban NM, Harvey S, Perrino FW, Hollis T. The structure of the mammalian RNase H2 complex provides insight into RNA??DNA hybrid processing to prevent immune dysfunction. J Biol Chem, 2010, 285:3617–24

510 37. Reijns MAM, Bubeck D, Gibson LCD, Graham SC, Baillie GS, Jones EY, Jackson AP.
511 The structure of the human RNase H2 complex defines key interaction interfaces
512 relevant to enzyme function and human disease. J Biol Chem, 2011, 286:10530–9
513 38. Lo MS. Monogenic Lupus. Curr Rheumatol Rep, 2016, 18:1–7
514 39. Figiel M, Chon H, Cerritelli SM, Cybulska M, Crouch RJ, Nowotny M. The structural
515 and biochemical characterization of human RNase H2 complex reveals the molecular
516 basis for substrate recognition and Aicardi-Goutières syndrome defects. J Biol Chem,
517 2011, 286:10540–50
518 40. Stein H, Hausen P. Enzyme from calf thymus degrading the RNA moiety of DNA-RNA
519 hybrids: Effect on DNA-dependent RNA polymerase. Science (80-), 1969, 166:393–5
520 41. Eder PS, Walder RY, Walder JA. Substrate specificity of human RNase H1 and its role
521 in excision repair of ribose residues misincorporated in DNA. Biochimie, 1993,
522 75:123–6
523 42. Crow YJ, Leitch A, Hayward BE, Garner A, Parmar R, Griffith E, Ali M, Semple C,
524 Aicardi J, Babul-Hirji R, Baumann C, Baxter P, Bertini E, Chandler KE, Chitayat D,
525 Cau D, Déry C, Fazzi E, Goizet C, King MD, Klepper J, Lacombe D, Lanzi G, Lyall H,
526 Martínez-Frías ML, Mathieu M, McKeown C, Monier A, Oade Y, Quarrell OW, Rittey
527 CD, Rogers RC, Sanchis A, Stephenson JBP, Tacke U, et al. Mutations in genes
528 encoding ribonuclease H2 subunits cause Aicardi-Goutières syndrome and mimic
529 congenital viral brain infection. Nat Genet, 2006, 38:910–6
530 43. Jensen KB, Driskell RR, Watt FM. Assaying proliferation and differentiation capacity of
531 stem cells using disaggregated adult mouse epidermis. Nat Protoc, 2010, 5:898–911
532 44. Ray A, Dittel BN. Isolation of mouse peritoneal cavity cells. J Vis Exp, 2010, 35:e1488
533 45. Lim JF, Berger H, Su IH. Isolation and activation of murine lymphocytes. J Vis Exp,
534 2016:54596
535 46. Durkin M, Qian X, Popescu N, Lowy D. Isolation of Mouse Embryo Fibroblasts. BIO-
536 PROTOCOL, 2013, 3
537 47. Hulley S, Cummings S, Browner W, Grady D, Newman T. Estimating Sample Size and

Power: Applications and Examples. Edited by Hulley S, Cummings S, Browner W, Grady D and Newman T. Des. Clin. Res. Fourth Edi, Philadelphia (PA), Lippincott Williams & Wilkins, 2013, pp. 55–83

48. Robinson PK. Enzymes: principles and biotechnological applications. Essays Biochem, 2015, 59:1–41

49. Copeland RA. Enzymes. A Practical Introduction to Structure, Mechanism and Data Analysis. 2nd ed. New York, Wiley-VCH, Inc., 2000. https://doi.org/10.1002/ange.19971091638

50. Magnusson B, Örnemark U. Eurachem Guide: The Fitness for Purpose of Analytical Methods – A Laboratory Guide to Method Validation and Related Topics. 2nd ed. Eurachem, 2014. https://doi.org/978-91-87461-59-0

51. Dowd JE, Riggs DS. A Comparison of Estimates of Michaelis-Menten Kinetic Constants From Various Linear Transformations. J Biol Chem, 1965, 240:863–9

52. Goods BA, Sansing L, Vahey JM, Christopher Love J, Steinschneider AF, Askenase MH. Correction to: blood handling and leukocyte isolation methods impact the global transcriptome of immune cells. BMC Immunol, 2018, 19:1–12

53. Grievink HW, Luisman T, Kluft C, Moerland M, Malone KE. Comparison of Three Isolation Techniques for Human Peripheral Blood Mononuclear Cells: Cell Recovery and Viability, Population Composition, and Cell Functionality. Biopreserv Biobank, 2016, 14:410–5

54. Chon H, Vassilev A, Depamphilis ML, Zhao Y, Zhang J, Burgers PM, Crouch RJ, Cerritelli SM. Contributions of the two accessory subunits, RNASEH2B and RNASEH2C, to the activity and properties of the human RNase H2 complex. Nucleic Acids Res, 2009, 37:96–110

55. Grützkau A, Radbruch A. Small but mighty: How the MACS1-technology based on nanosized superparamagnetic particles has helped to analyze the immune system within the last 20 years. Cytom Part A, 2010, 77:643–7

56. Smit JH, Van Der Velde JHM, Huang J, Trauschke V, Henrikus SS, Chen S,

Eleftheriadis N, Warszawik EM, Herrmann A, Cordes T. On the impact of competing intra- and intermolecular triplet-state quenching on photobleaching and photoswitching kinetics of organic fluorophores. Phys Chem Chem Phys, 2019, 21:3721–33

57. Torimura M, Kurata S, Yamada K, Yokomaku T, Kamataga Y, Kanagawa T, Kurane R. Fluorescence-Quenching Phenomenon by Photoinduced Electron Transfer between a Fluorescent Dye and a Nucleotide Base. Anal Sci, 2001, 17:155–60

58. Sakaue-Sawano A, Kurokawa H, Morimura T, Hanyu A, Hama H, Osawa H, Kashiwagi S, Fukami K, Miyata T, Miyoshi H, Imamura T, Ogawa M, Masai H, Miyawaki A. Visualizing Spatiotemporal Dynamics of Multicellular Cell-Cycle Progression. Cell, 2008, 132:487–98

578 ***Tables***

579 **Table 1**

buffer/ solution	reagents
RNase H2 assay reaction buffer (1x)	60 mM KCl, 50 mM Tris.HCl pH 8.0, 20 mM MgCl2, add fresh Triton X-100 and BSA to a final concentration of 0.01%
lysis buffer 1 (1x)	50 mM TRIS.HCL pH 8.0, 280 mM NaCl, 0,5% v/v NP40, 0,2 mM EDTA, 0,2 mM EGTA, 10% v/v glycerol, 0.1 mM sodium orthovanadate, add fresh 1 mM DTT and 1mM PMSF
lysis buffer 2 (1x)	20 mM HEPES, 10 mM KCl, 1 mM EDTA, 0.1 mM sodium orthovanadate, add fresh 1 mM DTT and 1mM PMSF

580

581 **Table 2**

RNase H2 assay substrates	sequence
oligonucleotide A: 2-O'-methylated RNA	5′-GAUCUGAGCCUGGGAGCU-fluorescein-3′
oligonucleotide B: DNA with a single ribounclotide	5′-GATCTGAGCCTGGG[rA]GCT-fluorescein-3'
oligonucleotide D: DNA	5''-Dabcyl-AGCTCCCAGGCTCAGATC-3'
oligonucleotide K: DNA	5′-AGCTCCCAGGCTCAGATC-3'

582

583 ***Figure descriptions***

584 **Figure 1 Assay principle and implementation of controls.**

585 **A)** RNase H2 activity assay design (adapted from Crow et al. [42]). Substrate BD, specific for
586 mammalian RNase H2 and bacterial RNase HII, is an 18 bp double-stranded DNA containing
587 a single ribonucleotide and a fluorescent residue (fluorescein) as well as a quencher (dabcyl)
588 on the complementary strand. RNase H2 cleavage at the position of the ribonucleotide
589 releases fluorescein from the quencher. Positive control substrates BK and B are identical
590 but lack the quencher or the complementary strand, respectively. RNase H2 does not cleave
591 single-stranded substrates like substrate B. Negative control substrate AD contains
592 methylated RNA resistant to RNase H2 and was used to control for substrate dequenching
593 by spontaneous dissociation.
594 **B)** Addition of 100U RNase HII lead to cleavage of positive control BK as well as substrate
595 BD with fluorescence reaching a plateau (BK plateau and BD plateau) above the
596 fluorescence levels of positive controls B and BK. This aligns with a quenching effect of the
597 complementary strand [56]. Positive control BK exceeded positive control B fluorescence when
598 no enzyme was added. This is explained with decreased fluorophore stability of substrate B
599 lacking the protective effect of the quenching complementary strand during storage [57]. Thus,
600 BD plateau fluorescence is the only valid positive control for calculation of substrate
601 cleavage. Fluorescence negative controls included quenched double-stranded substrate BD
602 without addition of RNase HII (BD no enzyme) and with addition of *heat-inactivated* cell
603 lysate (BD + *h.i.* lysate), quenched type 2 RNase H-resistant substrate (AD + RNase HII) and
604 blanks. Negative control fluorescence reached a maximum of 6.06 % (95 % CI: 5.26 % - 6.86
605 %) of BD plateau fluorescence. Unspecific substrate cleavage or degradation was
606 insignificant with 0.09 % per minute (95 % CI: 0.03 % / min - 0.15 % / min). Fluorophores
607 showed stable fluorescence with a fluorescence decrease of 1.68 % per hour (95%CI: 0.59
608 % / h - 2.78 % / h). Addition of lower amounts of RNase HII (e.g. 55 U, other curves are not

609 shown) yielded an increase in fluorescence with unexpectedly long lag phase before a hardly
610 definable steady state phase and a plateau phase.
611 **C)** Implementation of fluorescence standard curves revealed concentration-dependent
612 fluorescence non-linearity of the fluorophores. B and BD plateau fluorescence were
613 measured in triplicates at eight different substrate concentrations (20nM - 500nM) after
614 addition of 100 U RNase HII.
615 **D)** With help of the BD plateau fluorescence standard curve, fluorescence progress curves
616 were transformed into substrate cleavage progress curves now showing a perfectly linear
617 segment indicating steady-state conditions of the pseudo-first order irreversible cleavage
618 reaction.
619 **E)** A substrate conversion standard curve was implemented using different amounts of E.coli
620 RNase HII. Using this curve and quality controls, measured catalytic activity can be assigned
621 a standardized, externally validated unit ("eqU"). The curve showed no significant deviation
622 from linearity in the implemented assay working range (8.09 U – 200 U) (linear regression r
623 square = 0.99; Run's test: deviation from linearity not significant, P = 0.44).
624 **F)** Mean systematic error between separate RNase H2 assays performed under the same
625 assay conditions was 3.65 % (SD = 1.78; n = 3). The precision by which this systematic error
626 could be calculated was dependent on the number of quality controls used. Use of six
627 matched quality controls reduced variability of the calculation of systematic error to less than
628 3%.

629 Mean plus/ minus SD is shown.

630 **Figure 2 Ruggedness.**
631 **A)** Aliquots of the same sample were frozen at -20 °C and thawed up to 6 times. Each cycle
632 of freezing and thawing resulted in a mean activity loss of -0.37 eqU (Pearson's r = -0.94).
633 **B)** Aliquots of the same sample were stored at 26°C for up to 4 hours and activities were
634 compared with the RNase H2 assay. Mean loss of activity was -0.53 eqU/ hour (Pearson's r
635 = -0.91).

Figure 3 Steady-state kinetics.

The mean K_M was 141.7 nM (SEM = 27.86 %; 95 % CI: 69.4 – 213.9 nM). Calculation of K_M and V_{MAX} values showed high variability (C_V (K_M) = 65.72 %; C_V (V_{MAX}) = 24.45 %), while the C_V of individual measurements was dependent on the substrate concentration. RNase H2 activity at a substrate concentration of 270 nM (> 2 SD above K_M) was associated with a C_V below 10 % and implemented as assay end-point.

Mean ± SD is shown.

Figure 4 Assay precision.

RNase H2 activity was determined in lysates of mouse embryonic fibroblasts (MEFs), lysates of PBMCs isolated from human blood by Ficoll-Paque gradient centrifugation, lysates of HeLa cells (sorted for living cells via FACS) with normalization to total protein or cell number as indicated. Total assay variability of the different approaches is shown above the bars. Stacked colours indicate contributions of different error sources (cell isolation and preparation; cell/protein quantification; pipetting and measurement imprecision determined in separate experiments (not shown).

Figure 5 RNase H2 activity of different cell types.

Human induced pluripotent stem (iPS) cells, human embryonic kidney 293 cells (HEK293T), HeLa cells, human fibroblasts from the BJ cell line, human peripheral blood T cells ($CD3^+$) and B cells ($CD19^+$), murine spleen T cells ($CD4^+$), B cells ($CD19^+$), dendritic cells ($CD11b^+/CD11c^+$) and macrophages ($CD11b^+$), murine peritoneal macrophages ($F4/80^+$), murine epidermal stem cells ($CD49f^+$) and mouse embryonic fibroblasts (MEF) were purified and counted by flow cytometry. Cells were lysed, protein concentration was determined and RNase H2 activity was measured in biological triplicates under standard assay conditions.

A) RNase H2 activity normalized to cell number.

B) RNase H2 activity normalized to amount of total protein.

C) total cellular protein content of the cell types.

Mean ± SD is shown, significance was tested with the unpaired two tailed t-test, **** p < 0.0001, *** p < 0.001, ** p < 0.01 * p < 0.5, n.s. not significant.

Figure 6 Control group benchmarks.

A) RNase H2 activity normalized to total protein in T cells was significantly higher than in B cells.

B) RNase H2 activity normalized to cell number did not differ significantly, but showed significantly smaller variability in T cells.

C) Strong *inter*-individual variability was observed in B cells, while inter- and intra-individual variability were approximately on the same level as methodological error in T cells. Methodological variability was determined in validation experiments.

Median is shown, boxes indicate 25th and 75th percentile, whiskers indicating 10th and 90th percentile. Extreme outliers (>95th percentile oder < 5th percentile) are shown in the diagram, but were excluded for statistical testing. Normality could be assumed for all groups (Shapiro-Wilk test). Significance was tested via unpaired two tailed t-test, **** p < 0.0001, *** p < 0.001, ** p < 0.01 * p < 0.5, n.s. not significant.

Figure 7 RNase H2 activity in T cells from a patient carrying a heterozygous *RNASEH2C c.468G>T* variant.

A) Verification of the mutation by Sanger sequencing of DNA from PBMCs. The mutation is silent but affects the last base of exon 3, which is part of the splice donor site. This leads to aberrant splicing of the RNASEH2C mRNA, resulting in a sterile transcript [22].

B – D) RNase H2 activity normalized to cell number (B) or to total cellular protein (C) and total cellular protein content (D) of T cells heterozygous for the *RNASEH2C c.468G>T* variant compared to T cells from healthy controls (with unknown *RNASEH2* genotype, n=24).

Median is shown, boxes indicate 25th and 75th percentile, whiskers indicate 10th and 90th percentile, extreme outliers (>95th percentile oder < 5th percentile) are shown in the diagram, but were excluded for significance testing via unpaired two tailed t-test with Welch's correction, **** p < 0.0001, *** p < 0.001, ** p < 0.01 * p < 0.5, n.s. not significant.

689 ***Supplemental tables***

	cell type	minimum amount of protein/ well	maximum amount of protein/ well	optimal amount of protein/ well	number of cells yielding 1 µg total protein
murine	$CD4^+$ primary T cells	1.1	26.2	2.7 – 13.3	2.6E+04
	$CD11b^+$ spleen macrophages	2.9	70.6	7.2 – 35.8	8.2E+03
	$CD11b^+$/$CD11c^+$ spleen dendritic cells	2.8	67.2	6.8 – 34.1	5.8E+03
	$CD19^+$ primary B cells	1.3	32.6	3.3 – 16.6	9.7E+04
	$F4/80^+$ peritoneal macrophages	1.7	42.1	4.3 – 21.3	8.2E+03
	$CD49f^+$ epidermal stem cells	2.3	55.3	5.6 – 28.1	2.0E+04
	murine embryonic fibroblasts (MEFs)	8.6	210.2	21.3 – 106.7	1.4E+04

human	BJ cell line	32.1	782.4	79.4 – 397.1	2.4E+03
	HeLa cell line	0.9	23.1	2.3 – 11.7	4.3E+03
	HEK293T cell line	0.6	15.8	1.6 – 8.0	4.4E+03
	$CD3^+$ primary T cells	0.5	13.4	1.4 – 6.8	5.4E+04
	$CD19^+$ primary B cells	1.5	37.1	3.8 – 18.8	9.4E+03
	iPS cell line	0.5	13.1	1.3 – 6.7	1.0E+05

690

691 **Table S1 RNaseH2 assay working range for different cell types.**

692 Columns show minimum, maximum and recommended amount of total protein for each cell
693 type to achieve minimum (8.1 eqU), maximum (197 eqU) or optimal (> 20 eqU, < 100 eqU)
694 substrate conversion rates. The approximate number of cells needed for a yield of 1 µg of
695 total protein is shown on the right.

696

Descriptions for supplemental figures

Figure S1 Age and gender of the healthy control group (24 individuals with unknown RNASEH2 genotype). Median is shown, boxes indicate 25th and 75th percentile, whiskers indicate minimum and maximum.

Figure S2 Influence of cell cycle phase on RNase H2 activity.

FUCCI cell cycle reporter transgenic mice report cells in S / G2 / M phase of the cell cycle [58]. Total spleen cells of three FUCCI mice were isolated and stimulated in complete B cell medium for 48 hours with LPS (25 µg / ml) + IL-2 (180 U / ml), LPS (12.5 µg / ml) + IL-2 (180 U / ml) + PMA (5 ng / ml) or left untreated. Between 1x10^5 and 2x10^6 FUCCI$^+$ and FUCCI-negative CD19$^+$ B cells per mouse were sorted by FACS using anti-murine CD19 (eBio1D3) PE antibodies and RNase H2 activity was measured in triplicates.

A) Fraction of FUCCI$^+$ cells upon stimulation.

B) RNase H2 activity normalized to cell number in B cells in S / G2 / M-phase (FUCCI$^+$) versus FUCCI-negative B cells.

C) RNase H2 activity normalized to total cellular protein in B cells in S /G2 /M-phase (FUCCI$^+$) versus FUCCI-negative B cells.

D) Amount of protein per cell in B cells in S /G2 /M-phase (FUCCI$^+$) versus FUCCI$^-$ B cells. Cells stimulated with LPS and IL-2 possessed significantly more protein per cell than cells stimulated with LPS, IL-2 and PMA. FUCCI+ cells possessed significantly more cellular protein per cell than FUCCI-negative cells. Increase of cellular protein from FUCCI-negative to FUCCI+ cells was about 2.6-fold. Only stimulation with LPS + IL-2 significantly increased the amount of total cellular protein in FUCCI-negative cells.

Mean ± SD is shown, significance was tested via unpaired two tailed t-test, or 2-way ANOVA, as indicated in the graphs, **** $p < 0.0001$, *** $p < 0.001$, ** $p < 0.01$ * $p < 0.5$, n.s. not significant.

Figures:

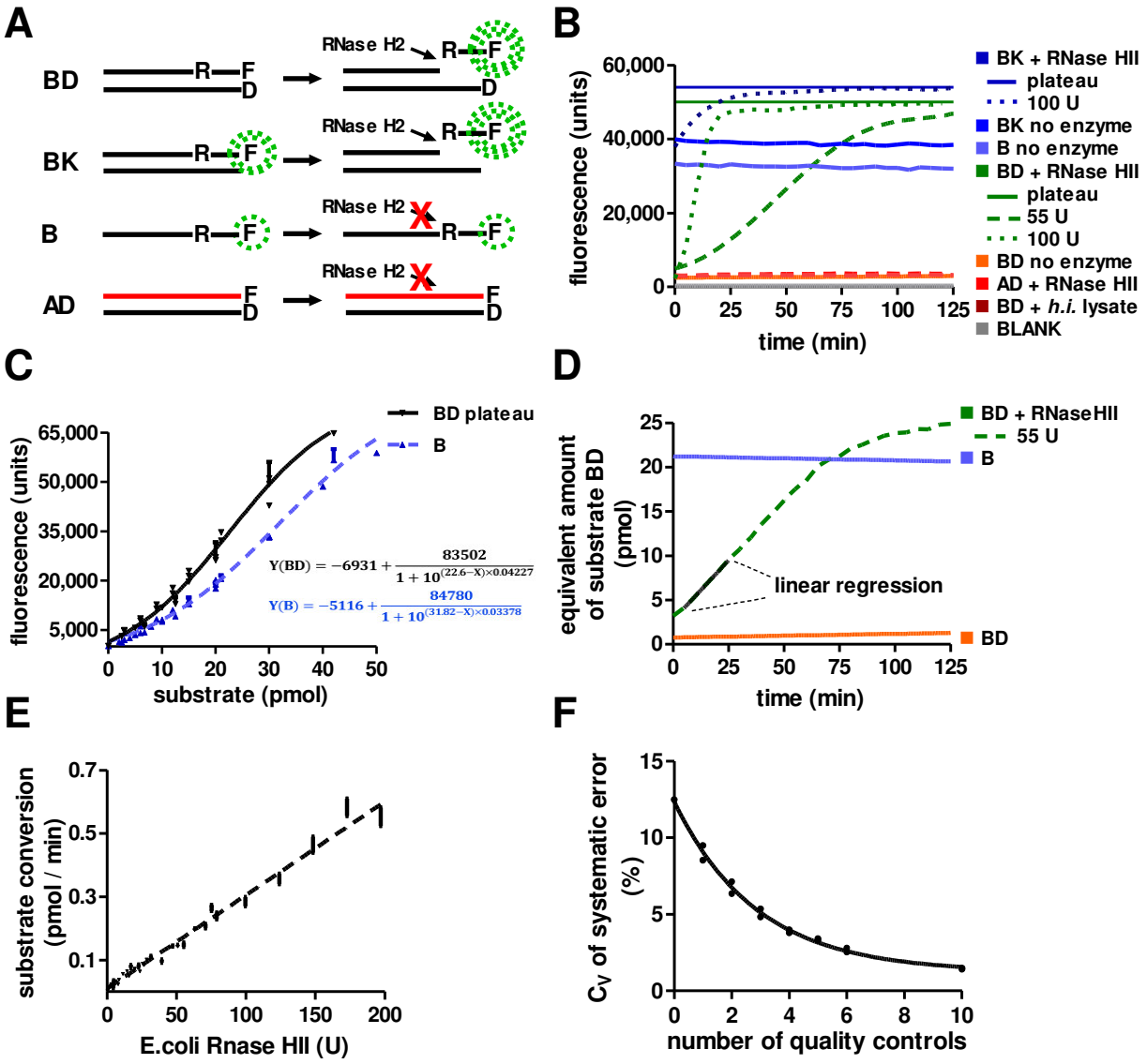

Figure 1

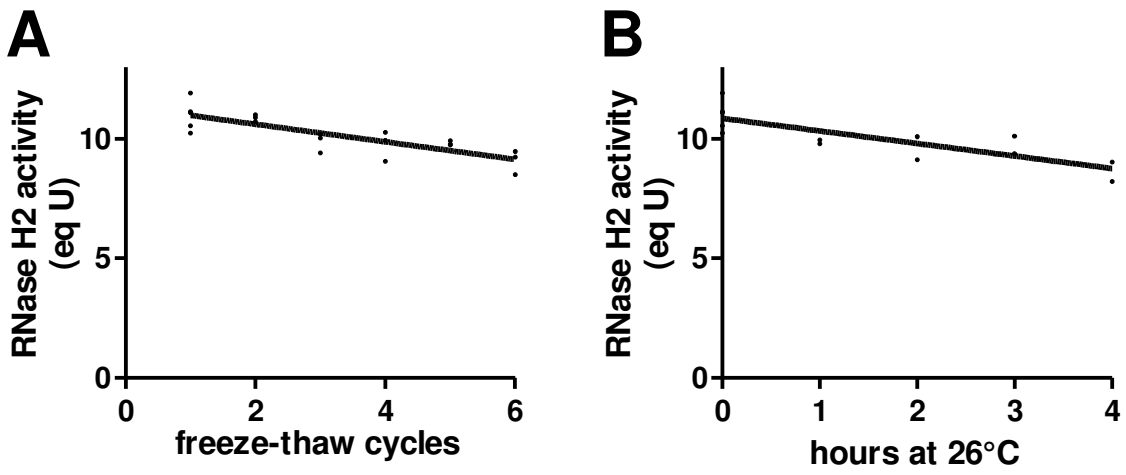

Figure 2

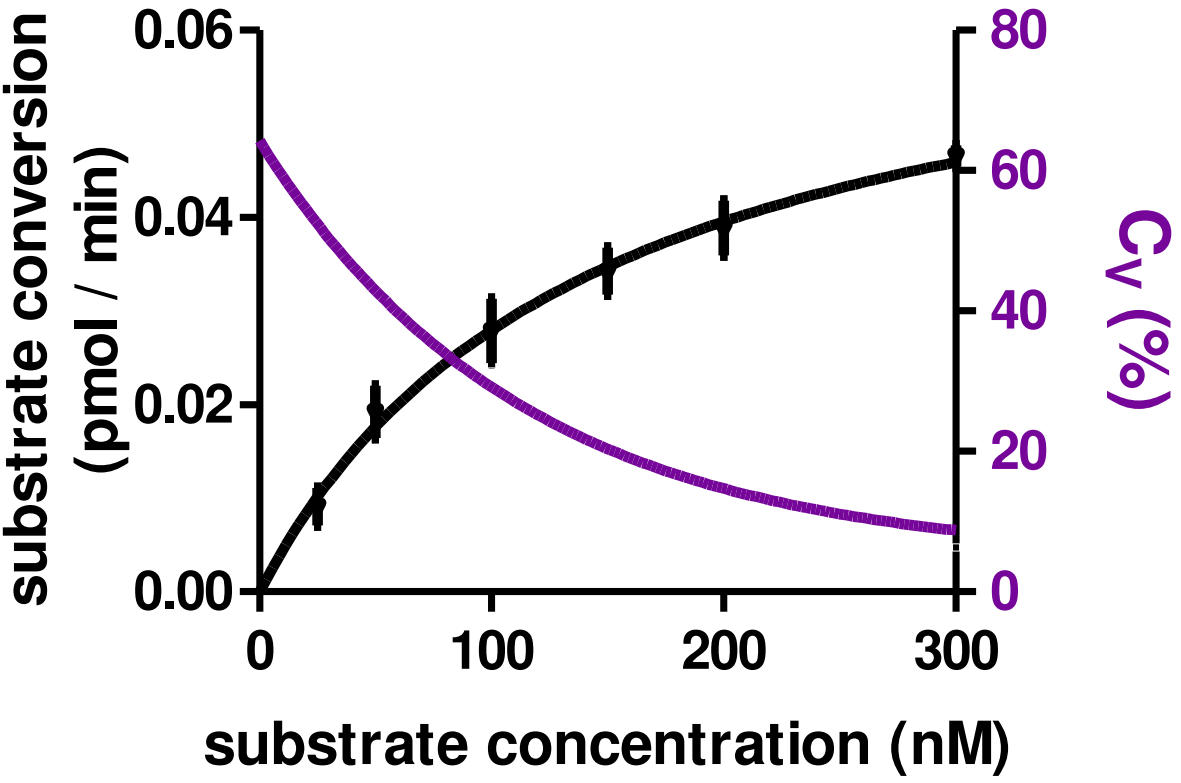

Figure 3

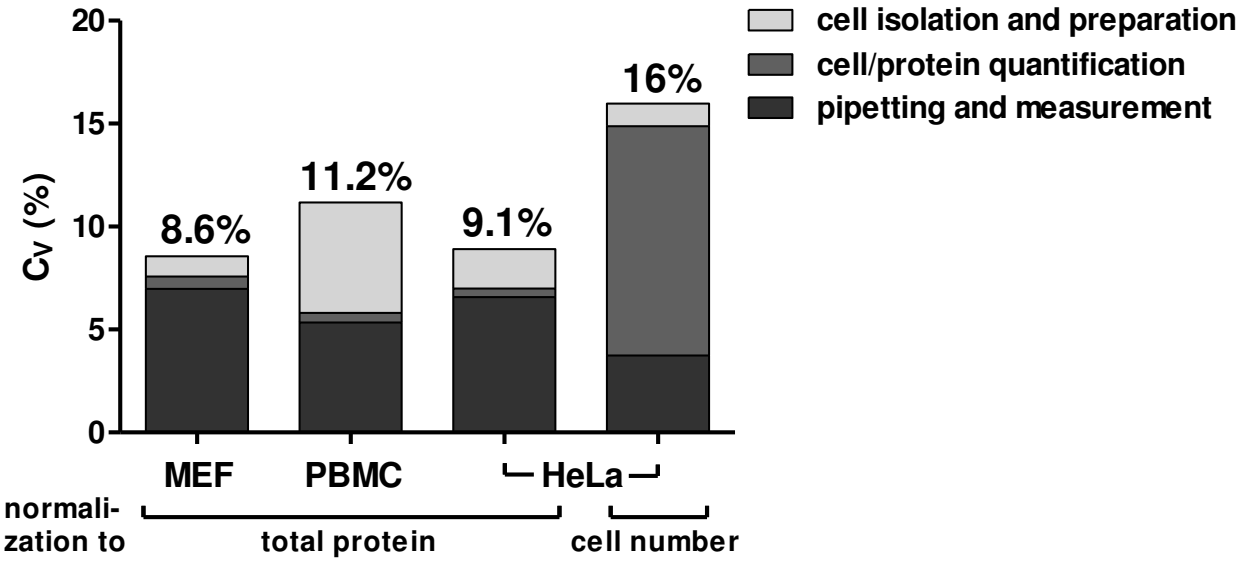

Figure 4

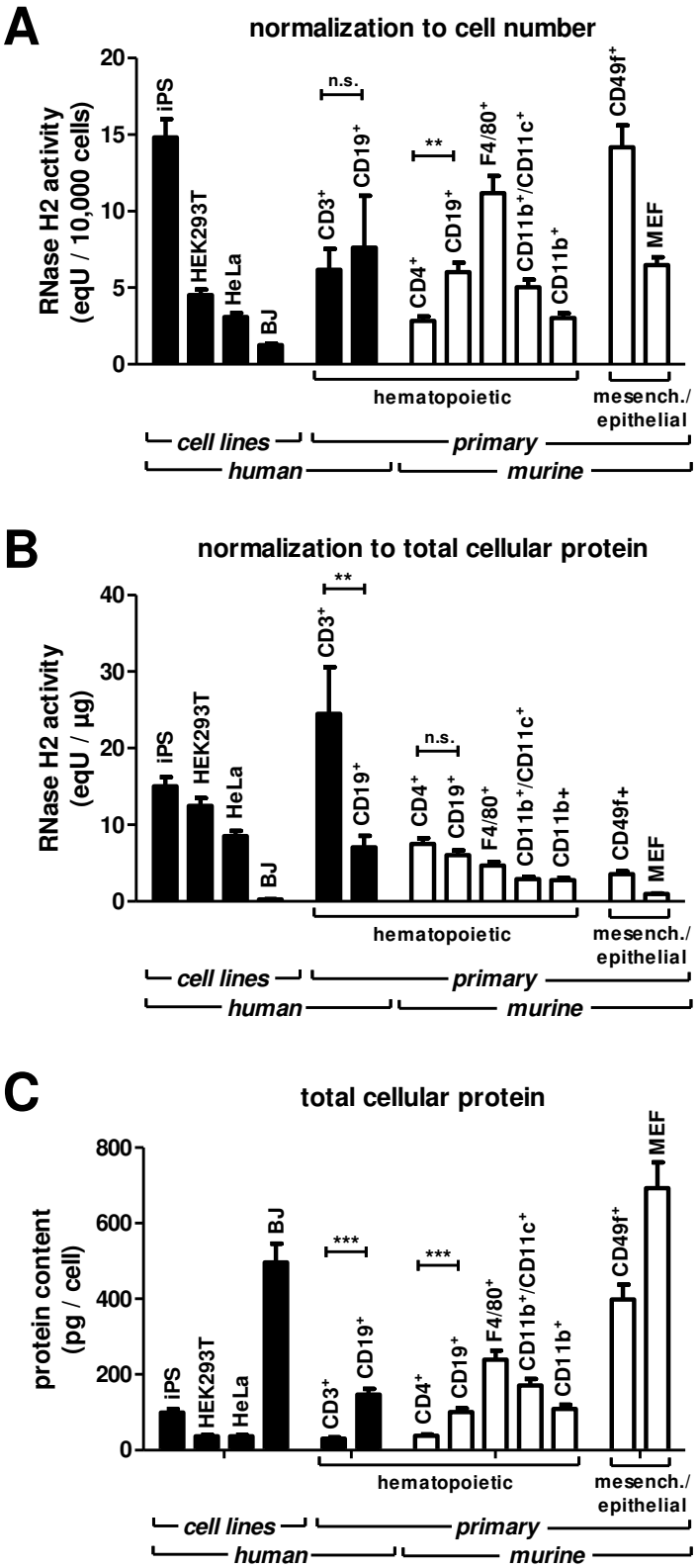

Figure 5

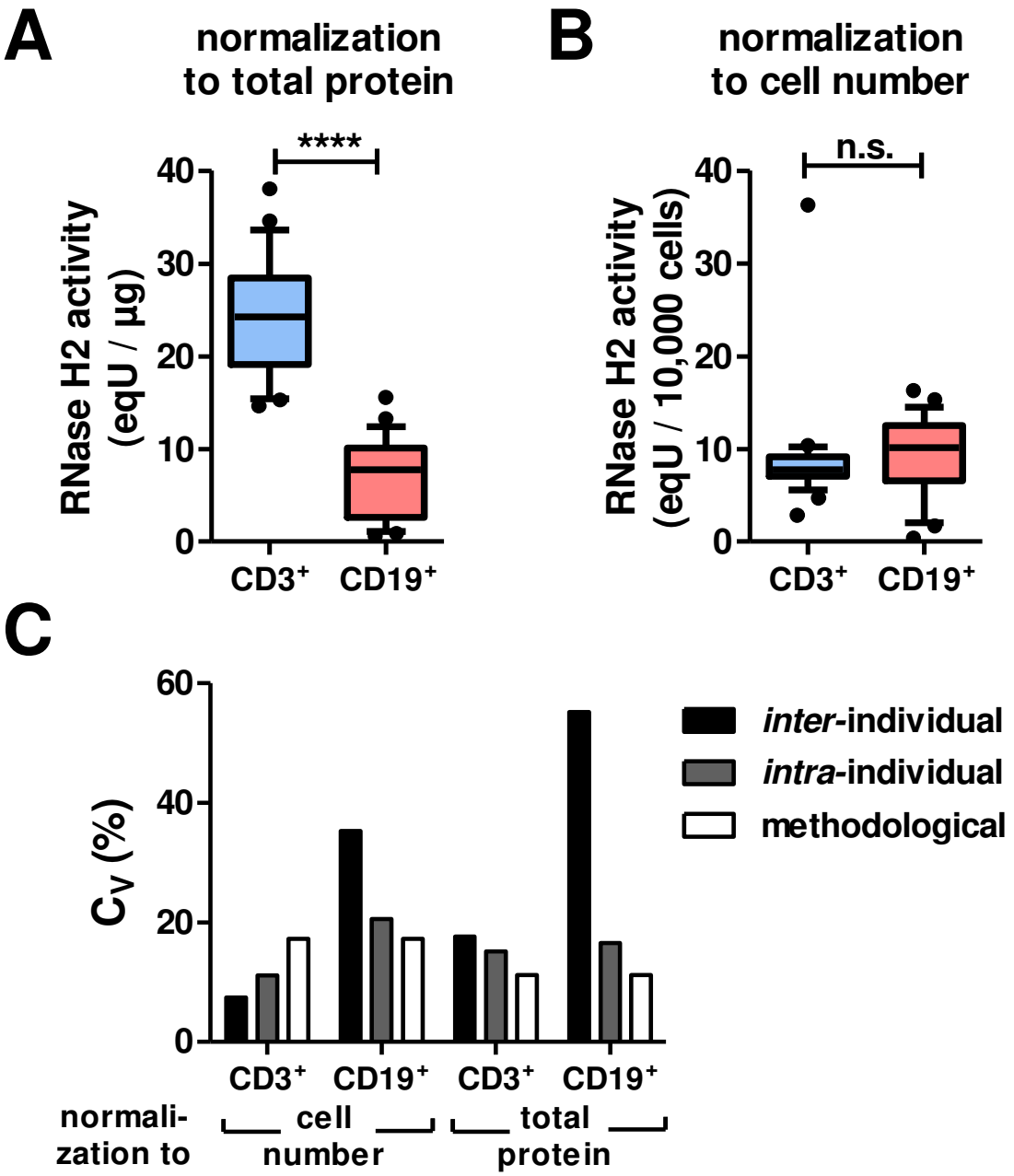

Figure 6

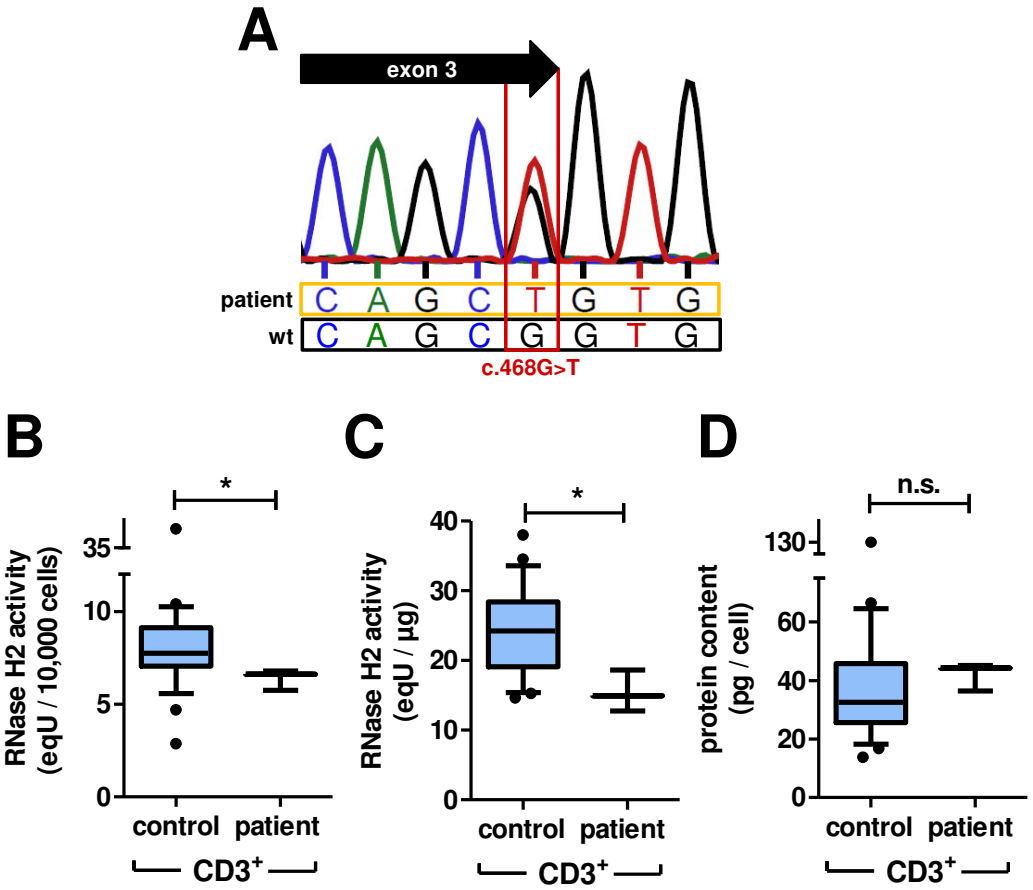

Figure 7

Supplemental figures:

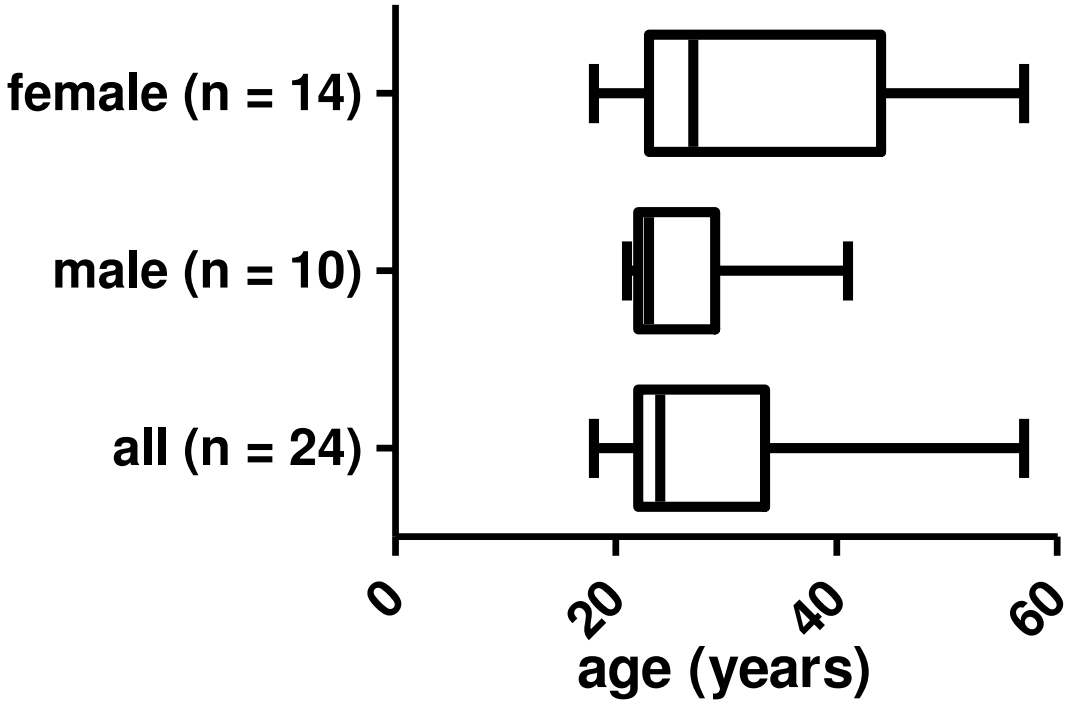

Figure S1

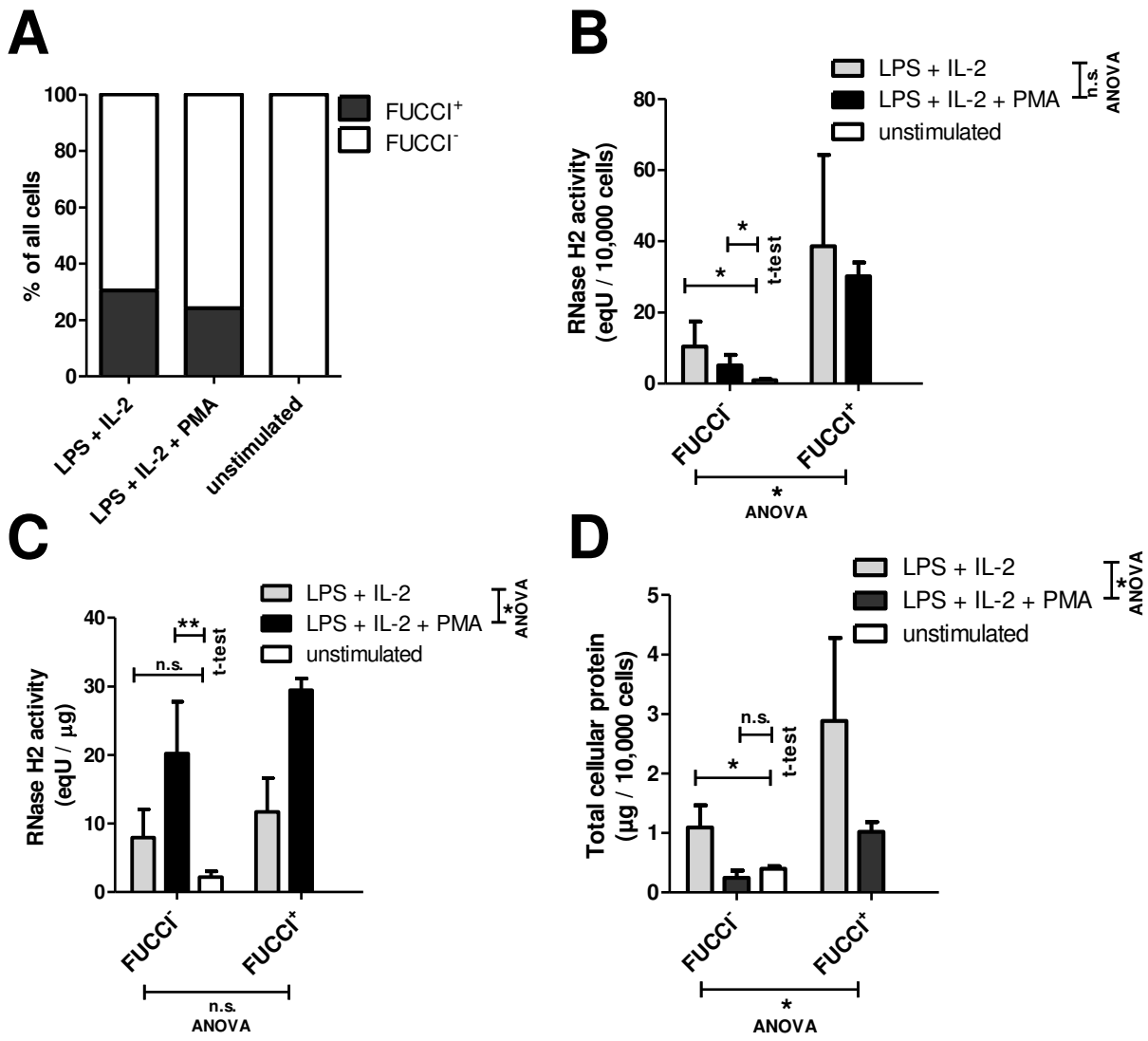

Figure S2